Frequency-Dependent Vortex Electromagnetic Wave Imaging

Guanqun Sun, Fangzheng Zhang, *Senior Member, IEEE*, and Shilong Pan, *Fellow, IEEE*

***Abstract*—Vortex electromagnetic (EM) wave radars provide a promising solution to forward-looking imaging with high azimuth resolution, while the previous systems require multiple radar pulses or complex hardware to transmit vortex EM waves carrying different orbital angular momentum (OAM) modes. To address this problem, a frequency-dependent vortex EM wave imaging method is proposed in this paper, in which frequency-dependent OAM modes carried by a single radar pulse are generated by a simple structure consisting of time delay units and a uniform circular array (UCA). In the receiver, an image construction method is proposed to address the frequency and OAM mode coupling, enabling fast imaging from a single radar pulse echo. A theoretical model is established, and numerical simulation is conducted to investigate the properties of frequency-dependent vortex EM waves and verify their feasibility for 2-D forward-looking imaging. The proposed method provides important technical support for efficient vortex EM wave imaging radars.**

***Index Terms*—Orbital angular momentum (OAM), radar imaging, vortex electromagnetic (EM) wave.**

I. Introduction

RADAR imaging is crucial for applications such as space target monitoring, remote sensing mapping, and ocean observation, etc. [1], [2]. Recently, vortex electromagnetic (EM) waves carrying orbital angular momentums (OAM) have gained significant interest because of their vortex-shaped phase front, offering a new degree of freedom in radar detection and imaging [3], [4], [5], [6]. This allows vortex EM wave radar to overcome the azimuth resolution limit in traditional forward-looking radars by exploiting the dual relation between OAM mode and azimuth angle [7], [8], [9], [10], [11], [12], [13], [14], [15], [16]. Hitherto, a lot of work has been conducted on the vortex EM wave radar, including imaging models and algorithms [17], [18], [19], [20], [21], [22], [23], as well as OAM beam steering methods [24], [25], [26].

Previously, most of the vortex EM wave radars employed a uniform circular array (UCA) and phased array technique to generate vortex EM waves. In these systems, each array channel has a phase shifter to introduce incremental phase shifts between adjacent channels. To generate different OAM modes, time-division multiplexing (TDM) technique is usually adopted to alter the phase shifts of the UCA at different radar pulses [5]. Consequently, in order to get a complete image frame, multiple radar pulses should be transmitted to encompass a broad OAM spectrum. This time-consuming process lowers the radar imaging speed and makes it difficult for imaging fast-moving targets. A possible solution is using multiring arrays to simultaneously generate vortex EM waves carrying different OAM modes, but this significantly increases the system complexity and cost, requiring specialized array designs [27], [28], [29].

Received 27 September 2024; accepted 14 October 2024. Date of publication 16 October 2024; date of current version 8 January 2025. This work was supported in part by the National Key Research and Development Program of China under Grant 2021YFB2800803, in part by the Natural Science Foundation of China under Grant 62371224, in part by the Natural Science Foundation of Jiangsu Province under Grant BK20221479, and in part by the Fundamental Research Funds for the Central Universities under Grant NS2023023. *(Corresponding author: Fangzheng Zhang.)*

The authors are with the College of Electronic and Information Engineering, Nanjing University of Aeronautics and Astronautics, Nanjing 210016, China (e-mail: zhangfangzheng@nuaa.edu.cn).

Digital Object Identifier 10.1109/LAWP.2024.3481634

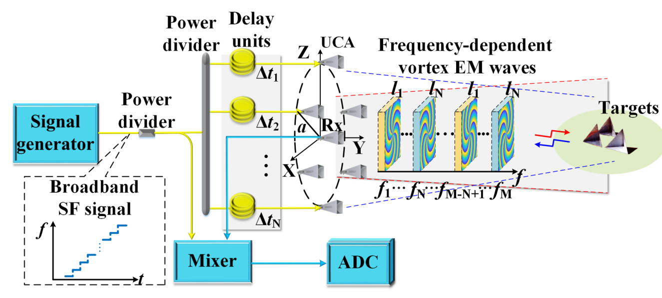

Fig. 1. Schematic diagram of the frequency-dependent vortex EM wave radar.

In this letter, we propose a frequency-dependent vortex EM wave imaging method that significantly enhances the efficiency of vortex EM wave radars. The system generates vortex EM waves with frequency-dependent OAM modes by a simple structure consisting of a set of time delay units and an UCA, enabling the transmission of multiple OAM modes within a single radar pulse. At the receiver, an image construction method is proposed to address the frequency and OAM mode coupling, allowing for fast imaging from a single radar pulse echo. A theoretical model of the proposed frequency-dependent vortex EM wave imaging is established. Numerical analyses are conducted to investigate the EM field characteristics of the frequency-dependent OAM beams, and target imaging is also simulated to verify the feasibility of forward-looking imaging with the proposed frequency-dependent vortex EM wave radar.

II. Principle

A. Frequency-Dependent Vortex EM Wave Radar

Fig. 1 shows the schematic diagram of the frequency-dependent vortex EM wave radar in which N transmit antennas compose an UCA and a single receive antenna (Rx) located at the center of the UCA is used to collect the echoes. In the transmitter, a broadband stepped-frequency (SF) signal is generated by an electrical signal generator. This SF signal contains M sub-pulses within one pulse, and it is expressed as

$$S_t(m,t) = rect\left(t/T_{pm}\right)\exp\left[j2\pi f_m t\right] \tag{1}$$

where $m = 0, 1, \ldots, M$-1. The term $rect(t/T_{\mathrm{pm}})$ represents a rectangular window with T_{pm} as the sub-pulse duration. In addition, $f_m = f_0 + m\Delta f$ is the frequency of the mth sub-pulse where f_0 is the initial frequency and Δf is the frequency step. This SF signal is divided into two branches by a 1×2 power divider. The upper branch is further divided into N channels using another $1 \times N$ power divider. Subsequently, N independent time delay units are used to introduce step-like time delays to the signals in different channels. Specifically, the time delay of the nth channel is $t_0 + n\Delta t$, where t_0 is the reference time delay and Δt is a fixed time delay step between adjacent channels. Here, the maximum delay difference $(N-1)\Delta t$ is controlled to be less than the sub-pulse duration T_{pm}, which ensures the signals transmitted by all the array elements have the same instantaneous frequency. In this case, the signal in the nth channel is given by

$$S_{tn}(m,t) = rect\left[\left(t+t_0+n\Delta t\right)/T_{pm}\right] \times e^{\left[j2\pi f_m\left(t+t_0+n\Delta t\right)\right]} \quad n = 0,1,\cdots,N-1. \tag{2}$$

In the 3-D coordinate system with the center of the UCA as the origin, the azimuth angle of the nth antenna is $\phi_n = 2\pi n/N$. When multichannel signals with a time delay step of Δt are transmitted by the UCA, the normalized electric field for the mth sub-pulse at position $P(r, \theta, \phi)$ in the far field is

$$E\left(m\right) = \sum_{n=0}^{N-1} \frac{e^{j2\pi f_m\left(t+t_0+n\Delta t-|\mathbf{r}-\mathbf{r}_n|/c\right)}}{|\mathbf{r}-\mathbf{r}_n|} \tag{3}$$

in which $\mathbf{r} = r \cdot \hat{\mathbf{r}}$, c is the propagation speed of the EM wave in the atmosphere and $\mathbf{r}_n$ denotes the position vector between position P and the nth antenna, with $\hat{\mathbf{r}}$ being the unit direction vector of $\mathbf{r}$. Based on the infinitesimal dipole approximation [6], the amplitude and phase of $|\mathbf{r}\text{-}\mathbf{r}_n|$ can be approximated as r and $r\text{-}a\sin\theta\cos(\phi\text{-}\phi_n)$, respectively, where a is the radius of the UCA. With these assumptions, the electric field in (3) can be approximately expressed as

$$\begin{aligned} E\left(m\right) &= \frac{1}{r}\sum_{n=0}^{N-1} e^{j2\pi f_m\left[t+t_0+n\Delta t-\left(r-a\sin\theta\cos\left(\phi-\phi_n\right)\right)/c\right]} \\ &= \frac{e^{j2\pi f_m\left(t+t_0-r/c\right)}}{r}\sum_{n=0}^{N-1} e^{j2\pi f_m a\sin\theta\cos\left(\phi-\phi_n\right)/c} e^{jn\Delta\psi\left(f_m\right)} \end{aligned} \tag{4}$$

where

$$\Delta\psi(f_m) = 2\pi f_m\Delta t. \tag{5}$$

Then, let

$$l(f_m) = \frac{\Delta\psi(f_m)}{2\pi/N} = \frac{2\pi f_m\Delta t}{2\pi/N} = N f_m\Delta t. \tag{6}$$

Equation (4) is rewritten as

$$\begin{aligned} E\left(m\right) &= \frac{e^{j2\pi f_m\left(t+t_0-r/c\right)}}{r}\sum_{n=0}^{N-1} e^{j\left[2\pi f_m a\sin\theta\cos\left(\phi-\phi_n\right)+l\left(f_m\right)\phi_n\right]} \\ &\approx \frac{Nj^{-l\left(f_m\right)}}{r} e^{j2\pi f_m\left(t+t_0-r/c\right)} e^{jl\left(f_m\right)\phi} J_{l\left(f_m\right)}\left(2\pi f_m a\sin\theta\right) \end{aligned} \tag{7}$$

in which $J_{l(fm)}(.)$ is the $l(f_m)$th-order Bessel function of the first kind. Derived from the phase term of $e^{jl(f_m)\phi}$, the emitted signal is a vortex EM wave carrying OAM and $l(f_{\mathrm{m}})$ is the OAM mode number. From (6), it is evident that the OAM mode of the generated vortex EM wave is jointly determined by the frequency f_m and the time delay step Δt. Since the time delay step Δt is fixed, the OAM mode carried by the vortex EM wave varies as the instantaneous frequency changes, i.e., the generated vortex EM wave is frequency-dependent.

In most cases, vortex EM wave radar uses integer OAM modes for image construction. To ensure that the generated vortex EM waves carry continuous integer OAM modes in the proposed system, the SF signal generator must be designed based on the following criteria:

$$l(f_0) = N f_0\Delta t \in \mathbb{Z},\ l(\Delta f) = N\Delta f\Delta t = 1 \tag{8}$$

where $\mathbb{Z}$ denotes the set of integers. Satisfying (8) requires

$$f_0 \in \frac{\mathbb{Z}}{N\Delta t}, \Delta f = \frac{1}{N\Delta t}. \tag{9}$$

On the other hand, the UCA possesses finite element number, which discretely samples the spatial phase around the circumference [30]. According to the Nyquist sampling theorem, the achievable integer OAM mode is constrained by the number of antenna elements, N, in the UCA, i.e.,

$$l = \begin{cases} \left\{l_1, l_2, \ldots, l_N \,\middle|\, -\frac{N-1}{2} \le l_n \le \frac{N-1}{2}, l_n \in \mathbb{Z}\right\}, & \text{if } N \text{ is odd} \\ \left\{l_1, l_2, \ldots, l_N \,\middle|\, -\frac{N}{2} \le l_n \le \frac{N}{2}-1, l_n \in \mathbb{Z}\right\}, & \text{if } N \text{ is even} \end{cases} \tag{10}$$

where l_1 and l_{N} represent the minimum and maximum OAM modes, respectively. Supposing the SF signal has a sufficiently large frequency sweeping range, the OAM mode of the generated vortex EM wave undergoes rapid periodic variations as the frequency is swept. Assuming that the OAM mode varies with a frequency period of η_f, the following equation should be satisfied

$$\begin{aligned} |l(f_m+\eta_f) - l(f_m)| &= \left|N\left(f_m+\eta_f\right)\Delta t - N\left(f_m\right)\Delta t\right| \\ &= N\eta_f\Delta t = N. \end{aligned} \tag{11}$$

Thus,

$$\eta_f = \frac{1}{\Delta t}. \tag{12}$$

B. Frequency-Dependent Vortex EM Wave Imaging

For conventional vortex EM radars, the targets are typically illuminated by multiple radar pulses carrying different OAM modes [5]. This indicates the image construction is done after transmitting and receiving multiple radar pulses. In contrast, the proposed frequency-dependent vortex EM radar transmits multiple OAM modes within a single radar pulse, enabling more efficient image construction from a single pulse echo. Assuming the target is composed of D scattering points. The scattering coefficient of the dth ($d = 1, 2,\cdots, D$) scattering point is β_d, and its location is (r_d, θ_d, ϕ_d). The echoes captured by the receive antenna can be expressed as

$$S_r\left(m\right) = Nj^{-l\left(f_m\right)}\sum_{d=1}^{D}\frac{\beta_m}{r_d r_d{}'} J_{l\left(f_m\right)}\left(2\pi f_m a\sin\theta_d\right) \times e^{j2\pi f_m\left(t+t_0-r_d-r_d{}'\right)/c} e^{jl\left(f_m\right)\phi_d} \tag{13}$$

where $r_d{}'$ is the distance between the dth scattering point and the receive antenna. To relax the hardware requirements, frequency down-conversion technique is employed to process the radar echoes [31], [32]. As shown in Fig. 1, the echoes are mixed with a reference SF signal from the lower branch of the 1×2 power divider, followed by digitization using an analog-to-digital converter (ADC). As shown in (13), the echo sample is

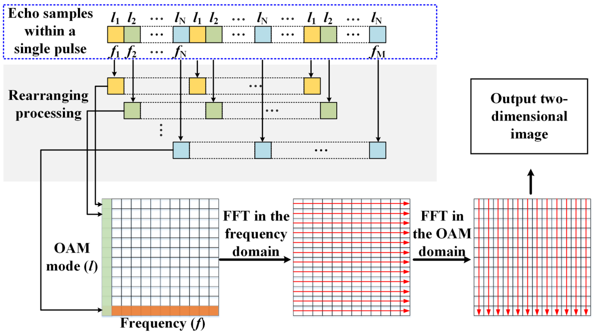

Fig. 2. Flowchart of the proposed image construction method.

a 1-D data with coupled information between frequency and OAM mode. This coupling makes it impossible for traditional imaging algorithms [10], [20], [21], [22], [23] to obtain the target profiles. To address this problem, an image construction method is proposed for the frequency-dependent vortex EM wave radar, as illustrated in Fig. 2.

In Fig. 2, a single pulse-echo contains M samples, each corresponding to a frequency-stepped sub-pulse, with OAM modes cyclically varying from l_1 to l_{N}. To decouple the 2-D information in frequency and OAM mode domains, data rearrangement is performed in such a way that the samples corresponding to the same OAM mode are selected to form a row vector and the obtained N row vectors are combined to construct a 2-D data matrix. In this matrix, columns represent the frequency dimension, and rows represent the OAM mode dimension. If the number of UCA antennas (N) is even, data for the OAM mode $l = -N/2$ should be discarded, as the phase of its EM wave no longer varies linearly with the azimuth angle. The rearranged 2-D data matrix can be regarded as the echo data acquired by a traditional vortex EM radar from different OAM mode pulses with a frequency step of η_f. Various imaging approaches, such as the fast Fourier transformation (FFT), power spectrum estimation, and compressive sensing can be applied to construct the image [20], [21], [22], [23]. In this letter, for the sake of verification and analysis, the conventional 2-D FFT method is employed in the frequency and OAM mode domains for the final image construction. Based on the FFT property [10], it is known that the range resolution ρ_{r} and the azimuth resolution ρ_θ for the frequency-dependent vortex EM wave radar satisfy

$$\rho_r = \frac{c}{2 \cdot \lfloor M/N \rfloor \cdot N\Delta f}, \; \rho_\theta = \frac{2\pi}{l_{num}} \tag{14}$$

where l_{num} is the number of effective OAM modes. Besides, the maximum unambiguous detection range $R_{\max}$ of radar can be derived based on the principle of SF radar detection [31] as

$$R_{\max} = \frac{c}{2\eta_f} = \frac{c \cdot \Delta t}{2}. \tag{15}$$

For the proposed frequency-dependent vortex EM wave radar including the image construction method, its prominent advantage is that vortex EM waves with different OAM modes are transmitted within a single radar pulse, enabling fast imaging with a simple system structure. Besides, according to (14) and (15), the performance metrics of the radar, such as resolution and unambiguous detection range, can be flexibly designed by adjusting the parameters of broadband SF signal, time delay units, and UCA to meet various application requirements. In practical applications, considering the large propagation losses and bandwidth limitation of electrical delay lines, low-loss analog optical links can be applied in the system to provide large time delays [33], [34], [35].

TABLE I
PARAMETER DESIGN OF FREQUENCY-DEPENDENT VORTEX EM WAVE RADAR

Parameter	Symbol	Value
Initial frequency	f_0	9 GHz
Bandwidth	B	2 GHz
Frequency step	Δf	0.2 MHz
Antenna number	N	16
Array radius	a	0.1 m
OAM mode	l	[-8, 7]
Time delay step	Δt	312.5 ns

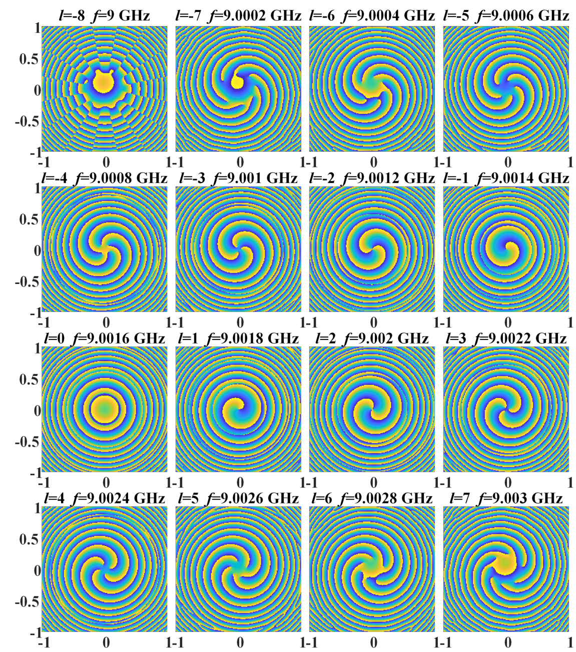

Fig. 3. Phase distributions for 16 sub-pulses at different frequencies.

III. SIMULATIONS

In this section, simulations are conducted to validate the effectiveness of the proposed frequency-dependent vortex EM wave generation and image construction method. The key parameters utilized in these simulations are listed in Table I.

First, the EM field characteristics of the frequency-dependent OAM beams are investigated. According to (10), (12), and the parameters in Table I, the OAM modes periodically vary from −8 to 7 as the frequency sweeps, with a frequency period of 3.2 MHz. Given that the initial frequency f_0, frequency step Δf, and time delay step Δt satisfy the criteria in (8) and (9), the generated vortex EM waves carry continuous integer OAM modes with a spacing of 1. For analysis, we selected 16 sub-pulses of the first OAM mode variation period to check their radiation characteristics. The EM field is observed along a cross-section parallel to the xoz-plane at a distance of 2 m. The observation window is 2 m wide in both x- and z-directions. Fig. 3 illustrates the phase distributions for sub-pulses at different frequencies, confirming that the proposed structure successfully generates vortex EM waves with multiple integer OAM modes within a single pulse. To further analyze the frequency-dependent vortex EM wave characteristics, the OAM spectrum is calculated via mode decomposition by performing Fourier transformation on the observed azimuth phase [36]. Fig. 4 shows the OAM

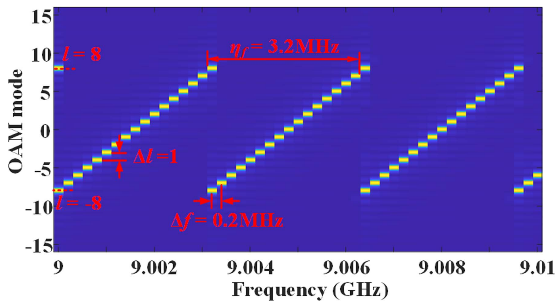

Fig. 4. OAM spectrum in a 100 MHz range (from 9 GHz to 9.01 GHz).

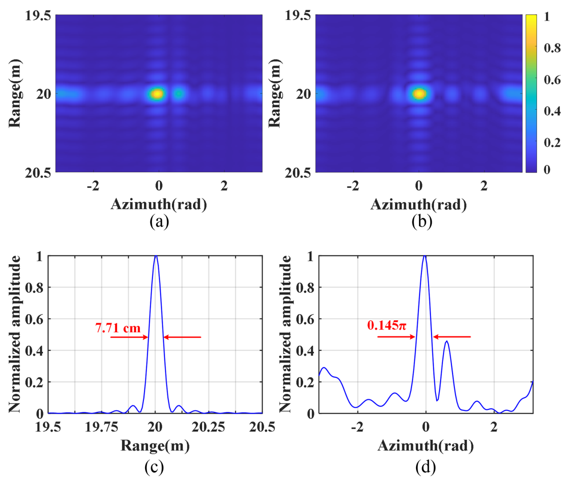

Fig. 5. (a) Single-point target image obtained by frequency-dependent vortex EM wave radar. (b) Image obtained by traditional vortex EM radar. (c) Range profile and (d) azimuth profile of the target in (a).

spectrum within a 100 MHz frequency range (9 GHz to 9.01 GHz). It should be noted that, for vortex EM wave generation with a 16-element UCA, the OAM mode with $l = 8$ is actually the same with the OAM mode with $l = -8$. Thus, the OAM modes in Fig. 4 exhibit periodic variation from $l = -8$ to $l = 7$ with a total number of 16. It is also known from Fig. 4 that the frequency period as the OAM mode changes from $l = -8$ to $l = 7$ is 3.2 MHz. Thus, the OAM modes variation properties are consistent with theoretical analysis.

Then, numerical simulations are conducted to validate the effectiveness of 2-D imaging by the frequency-dependent vortex EM wave radar. According to (15), the parameters lead to a maximum unambiguous detection range of 46.84 m. An ideal point target located at (20 m, 0.175, 0) is first imaged. The target is illuminated with the generated frequency-dependent vortex EM waves carrying 16 OAM modes within a single radar pulse. In the receiver, the radar echoes are down-converted and digitalized to obtain one sample per sub-pulse. For a single radar pulse echo, there are 10 000 samples in total, which are rearranged into 16 sets corresponding to different OAM modes. Since the OAM mode with $l = -8$ lacks a vortex-shaped phase front, its data is discarded, leaving 15 effective OAM modes. The remaining data is rearranged into a 15 (OAM mode) × 625 (frequency) matrix, and 2-D FFT is applied to obtain the range-azimuth image. Fig. 5(a) shows that the target is accurately constructed at ($r = 20$ m, $\phi = 0$). For comparison, traditional vortex EM radar imaging is also simulated, in which 15 radar pulses carrying different OAM modes ranging from −7 to 7 are sequentially transmitted to illuminate the target and received by the receiver. Each pulse starts at 9 GHz, having a frequency step of 3.2 MHz and a total bandwidth of 2 GHz. The image constructed using 2-D FFT method is shown in Fig. 5(b). By comparing the images in Fig. 5(a) and (b), it is found that the proposed frequency-dependent vortex EM radar achieves imaging quality and signal-to-noise ratio comparable to the traditional vortex EM radar, while the transmission and reception of multiple OAM modes are greatly simplified. To analyze the imaging resolution using the proposed vortex EM radar imaging method, Fig. 5(c) and (d) presents the range and azimuth profiles of the target in the Fig. 5(a). The full widths at half maximum of the range and azimuth profiles are measured to be 7.71 cm and 0.145π, respectively, closely matching the theoretical values of 7.49 cm and 0.134π from (14). However, the FFT-based image exhibits obvious sidelobes, particularly in the frequency-dependent vortex EM radar. This is caused by the frequency difference of Δf between adjacent data in the same column of the rearranged 2-D data matrix. To address this issue, a windowing technique can be applied to the 2-D data matrix along the OAM mode dimension before performing FFT [11].

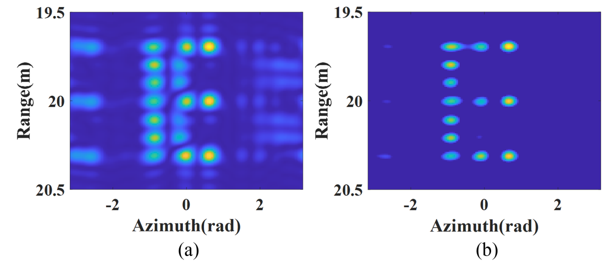

Fig. 6. (a) Constructed images of the E-shaped complex target using the FFT method. (b) Imaging result when applying Kaiser window.

Next, the imaging of a complex E-shaped target is demonstrated. The target consists of 13 points located at (19.7 m, −0.8), (19.8 m, −0.8), (19.9 m, −0.8), (20 m, −0.8), (20.1 m, −0.8), (20.2 m, −0.8), (20.3 m, −0.8), (19.7 m, 0), (20 m, 0), (20.3 m, 0), (19.7 m, 0.8), (20 m, 0.8), and (20.3 m, 0.8) in the range-azimuth plane, and their elevations being 0.175. Fig. 6(a) shows the image constructed by 2-D FFT without windowing. While the E-shaped profile is visible, sidelobes significantly affect the image quality. To mitigate this, Kaiser windowing is used along the OAM mode dimension with the result shown in Fig. 6(b). Since the sidelobes are effectively suppressed, the 13 points are much better focused in the high-contrast image shown in Fig. 6(b), which allows the features of the E-shaped target to be clearly recognized. Therefore, the frequency-dependent vortex EM wave imaging is competent for imaging of complex targets and it can be applied in real applications.

IV. Conclusion

In conclusion, we have proposed and demonstrated a frequency-dependent vortex EM wave imaging method that improves the efficiency of traditional vortex EM wave radars. This method uses a simple system structure to transmit different OAM modes within a single radar pulse and constructs images from a single radar pulse echo. Through theoretical analysis and simulations, characteristics of the frequency-dependent vortex EM waves are investigated and the feasibility of the 2-D imaging capability is verified. This method can promote the development of vortex EM wave imaging techniques and improve its practical application ability.

References

[1] D. A. Ausherman, A. Kozma, J. L. Walker, H. M. Jones, and E. C. Poggio, "Developments in radar imaging," *IEEE Trans. Aerosp. Electron. Syst.*, vol. AES-20, no. 4, pp. 363–400, Jul. 1984.

[2] D. Bleh et al., "W-band time-domain multiplexing FMCW MIMO radar for far-field 3-D imaging," *IEEE Trans. Microw. Theory Techn.*, vol. 65, no. 9, pp. 3474–3484, Sep. 2017.

[3] J. D. Jackson, *Classical Electrodynamics*, 3rd ed. New York, NY, USA: Wiley, 1998.

[4] R. Chen, H. Zhou, M. Moretti, X. Wang, and J. Li, "Orbital angular momentum waves: Generation, detection and emerging applications," *IEEE Commun. Surveys Tuts.*, vol. 22, no. 2, pp. 840–868, 2nd Quarter 2020.

[5] K. Liu, Y. Cheng, X. Li, and Y. Gao, "Microwave-sensing technology using orbital angular momentum: Overview of its advantages," *IEEE Veh. Technol. Mag.*, vol. 14, no. 2, pp. 112–118, Jun. 2019.

[6] S. M. Mohammadi et al., "Orbital angular momentum in radio—A system study," *IEEE Trans. Antennas Propag.*, vol. 58, no. 2, pp. 565–572, Feb. 2010.

[7] Y. Zhu, Y. Zhou, Y. Chen, L. Bu, and H. Zhao, "A mode optimization method for vortex electromagnetic wave radar imaging," *IEEE Geosci. Remote Sens. Lett.*, vol. 19, pp. 1–5, 2022.

[8] J. Liang, Q. Zhang, Y. Luo, H. Yuan, and Y. Chen, "Three-dimensional imaging with bistatic vortex electromagnetic wave radar," *Remote Sens.*, vol. 14, no. 13, Jun. 2022, Art. no. 2972.

[9] L. Li and F. Li, "Beating the Rayleigh limit: Orbital-angular-momentum-based super-resolution diffraction tomography," *Phys. Rev. E, Statist. Phys. Plasmas Fluids Relat. Interdiscip. Top.*, vol. 88, no. 3, Sep. 2013, Art. no. 033205.

[10] K. Liu, Y. Cheng, Z. Yang, H. Wang, Y. Qin, and X. Li, "Orbital-angular-momentum-based electromagnetic vortex imaging," *IEEE Antennas Wireless Propag. Lett.*, vol. 14, pp. 711–714, 2015.

[11] K. Liu, Y. Cheng, Y. Gao, X. Li, Y. Qin, and H. Wang, "Super-resolution radar imaging based on experimental OAM beams," *Appl. Phys. Lett.*, vol. 110, no. 16, Apr. 2017, Art. no. 164102.

[12] T. Yang, H. Shi, J. Guo, and D. Liu, "3D sparse ISAR imaging with multiple plane spiral OAM electromagnetic waves," *IEEE Sensors J.*, vol. 22, no. 15, pp. 15082–15097, Aug. 2022.

[13] D. Orfeo et al., "Ultra-wideband ground penetrating radar with orbital angular momentum control," *Proc. SPIE*, vol. 11750, Apr. 2021, Art. no. 1175007.

[14] H. Qu, S. Li, C. Chen, J. Liu, and W. Chen, "High-resolution orbital angular momentum imaging with the removal of bessel function modulation effect," *IEEE Trans. Microw Theory Techn.*, vol. 72, no. 4, pp. 2577–2590, Apr. 2024.

[15] G. Sun, F. Zhang, K. Zhao, and S. Pan, "Photonics-based broadband vortex electromagnetic wave generation for high-resolution imaging," *J. Lightw. Technol.*, vol. 42, no. 6, pp. 1894–1900, Mar. 2024.

[16] G. Sun et al., "Photonics-based broadband single-input-multiple-output OAM coincidence imaging," *IEEE Trans. Radar Syst.*, vol. 2, pp. 690–698, Jun. 2024.

[17] H. Liu, Y. Wang, J. Wang, K. Liu, and H. Wang, "Electromagnetic vortex enhanced imaging using fractional OAM beams," *IEEE Antennas Wireless Propag. Lett.*, vol. 20, no. 6, pp. 948–952, Jun. 2021.

[18] H. Liu, K. Liu, Y. Cheng, and H. Wang, "Microwave vortex imaging based on dual coupled OAM beams," *IEEE Sensors J.*, vol. 20, no. 2, pp. 806–815, Jan. 2020.

[19] K. Liu, Y. Cheng, X. Li, and Y. Jiang, "Passive OAM-based radar imaging with single-in-multiple-out mode," *IEEE Microw. Wireless Compon. Lett.*, vol. 28, no. 9, pp. 840–842, Sep. 2018.

[20] K. Liu, Y. Cheng, X. Li, Y. Qin, H. Wang, and Y. Jiang, "Generation of orbital angular momentum beams for electromagnetic vortex imaging," *IEEE Antennas Wireless Propag. Lett.*, vol. 15, pp. 1873–1876, 2016.

[21] S. Guo, Z. He, and R. Chen, "High resolution 2-D electromagnetic vortex imaging using uniform circular arrays," *IEEE Access*, vol. 7, pp. 132430–132437, 2019.

[22] R. Li, Z. Ma, Q. Zhang, Y. Luo, B. Liang, and G. Li, "Sparse-Bayesian-learning-based translational motion estimation of electromagnetic vortex imaging," *J. Eng.*, vol. 2019, no. 21, pp. 8002–8005, Nov. 2019.

[23] H. Zhao and K. Wang, "Orbital-angular-momentum-based radar imaging by dice regularized orthogonal matching pursuit," in *Proc. IEEE 5th Int. Conf. Signal Image Process.*, Oct. 2020, pp. 446–450.

[24] T. Yuan, Y. Cheng, H. Wang, and Y. Qin, "Beam steering for electromagnetic vortex imaging using uniform circular arrays," *IEEE Antennas Wireless Propag. Lett.*, vol. 16, pp. 704–707, 2017.

[25] T. Yuan, H. Wang, Y. Qin, and Y. Cheng, "Electromagnetic vortex imaging using uniform concentric circular arrays," *IEEE Antennas Wireless Propag. Lett.*, vol. 15, pp. 1024–1027, 2016.

[26] K. Liu, H. Wang, H. Liu, Y. Cheng, and X. Li, "Orbital angular momentum imaging based on waveform diversity and rotational array," *IEEE Trans. Microw. Theory Techn.*, vol. 71, no. 6, pp. 2714–2720, Jun. 2023.

[27] D. Liu, L. Gui, Z. Zhang, H. Chen, G. Song, and T. Jiang, "Multiplexed OAM wave communication with two-OAM-mode antenna systems," *IEEE Access*, vol. 7, pp. 4160–4166, 2019.

[28] F. Qin, L. Li, Y. Liu, W. Cheng, and H. Zhang, "A four-mode OAM antenna array with equal divergence angle," *IEEE Antennas Wireless Propag. Lett.*, vol. 18, no. 9, pp. 1941–1945, Sep. 2019.

[29] D. Lee, H. Sasaki, H. Fukumoto, Y. Yagi, and T. Shimizu, "An evaluation of orbital angular momentum multiplexing technology," *Appl. Sci.*, vol. 9, no. 9, Apr. 2019, Art. no. 1729.

[30] T. Yuan, Y. Cheng, H. Wang, and Y. Qin, "Mode characteristics of vortical radio wave generated by circular phased array: Theoretical and experimental results," *IEEE Trans. Antennas Propag.*, vol. 65, no. 2, pp. 688–695, Feb. 2017.

[31] W. Su, M. Tang, R. E. Arif, T. Horng, and F. Wang, "Stepped-frequency continuous-wave radar with self-injection-locking technology for monitoring multiple human vital signs," *IEEE Trans. Microw. Theory Techn.*, vol. 67, no. 12, pp. 5396–5405, Dec. 2019.

[32] D. Schindler, B. Schweizer, C. Knill, J. Hasch, and C. Waldschmidt, "An integrated stepped-carrier OFDM MIMO radar utilizing a novel fast frequency step generator for automotive applications," *IEEE Trans. Microw. Theory Techn.*, vol. 67, no. 11, pp. 4559–4569, Jun. 2019.

[33] C. Cox, *Analog Optical Links: Theory and Practice*. Cambridge, MA, USA: Cambridge Univ. Press, 2004.

[34] D.-H. Shin, D.-H. Jung, D.-C. Kim, J.-W. Ham, and S.-O. Park, "A distributed FMCW radar system based on fiber-optic links for small drone detection," *IEEE Trans. Instrum. Meas.*, vol. 66, no. 2, pp. 340–347, Feb. 2017.

[35] G. Serafino et al., "Toward a new generation of radar systems based on microwave photonic technologies," *J. Lightw. Technol.*, vol. 37, no. 2, pp. 643–650, Jan. 2019.

[36] R. Mao, K. Liu, H. Liu, Y. Yang, and H. Xiao, "Electromagnetic vortex imaging based on OAM multiplexing beam with orthogonal polyphase coding," *IEEE Sens. J.*, vol. 23, no. 24, pp. 30786–30793, Dec. 2023.